HHS Public Access

Author manuscript

Biofabrication. Author manuscript; available in PMC 2023 November 18.

Published in final edited form as:

Biofabrication. ; 15(1): . doi:10.1088/1758-5090/ac9f70.

Comparison of In-Situ versus Ex-Situ Delivery of Polyethylenimine-BMP-2 polyplexes for Rat Calvarial Defect Repair via Intraoperative Bioprinting

Kazim K. Moncal[1,2,3,#], **Miji Yeo**[1,2,#], **Nazmiye Celik**[1,2], **Timothy M. Acri**[4], **Elias Rizk**[5], **Hwabok Wee**[1,6], **Gregory S. Lewis**[1,6], **Aliasger K. Salem**[4,7], **Ibrahim T. Ozbolat**[1,2,5,8,9,10,*]

[1]Engineering Science and Mechanics, Pennsylvania State University, University Park, PA, USA

[2]Huck Institutes of the Life Sciences, Pennsylvania State University, University Park, PA, USA

[3]Molecular Imaging Program at Stanford (MIPS), Department of Radiology, Stanford University, Stanford, CA, USA

[4]Division of Pharmaceutics and Translational Therapeutics, Collage of Pharmacy, University of Iowa, Iowa City, IA, USA

[5]Department of Neurosurgery, Penn State University, College of Medicine, Hershey, PA, USA

[6]Department of Orthopedics and Rehabilitation, Penn State University, College of Medicine, Hershey, PA, USA

[7]Department of Chemical and Biochemical Engineering, College of Engineering, University of Iowa, Iowa City, IA, USA

[8]Biomedical Engineering, Pennsylvania State University, University Park, PA, USA

[9]Materials Research Institute, Pennsylvania State University, University Park, PA, USA

[10]Department of Medical Oncology, Cukurova University, Adana, Turkey

Abstract

Gene therapeutic applications combined with bio- and nano-materials have been used to address current shortcomings in bone tissue engineering due to their feasibility, safety and potential capability for clinical translation. Delivery of non-viral vectors can be altered using gene-activated matrices to improve their efficacy to repair bone defects. Ex-situ and in-situ delivery strategies are the most used methods for bone therapy, which have never been directly compared for their

*Corresponding author: ito1@psu.edu.

#Contributed equally

Author Contributions

K.K.M., M.Y. and I.T.O. developed the ideas and designed the experimental plan. T.M.A. produced pDNAs and performed particle size and zeta potential characterization. K.K.M. performed transfection of particles, cell culture, bioink preparation, IOB of bone, animal handling, cryosectioning, histomorphometric characterizations, staining and imaging. M.Y. performed in vitro studies. N.C. supported to generate the RT-PCR data. E.R. performed animal surgeries. H. W. performed μCT scanning and analyzed the data with G.S.L. All the authors contributed to the manuscript writing.

Conflict of interest

I T O has an equity stake in Biolife4D and is a member of the scientific advisory board for Biolife4D and Brinter. Other authors confirm that there are no known conflicts of interest associated with this publication and there has been no significant financial support for this work that could have influenced its outcome.

potency to repair critical-sized bone defects. In this regard, we first time explore the delivery of polyethylenimine (PEI) complexed plasmid DNA encoding bone morphogenetic protein-2 (PEI-pBMP-2) using the two delivery strategies, ex-situ and in-situ delivery. To realize these gene delivery strategies, we employed intraoperative bioprinting (IOB), enabling us to 3D bioprint bone tissue constructs directly into defect sites in a surgical setting. Here, we demonstrated IOB of an osteogenic bioink loaded with PEI-pBMP-2 for the in-situ delivery approach, and PEI-pBMP-2 transfected rat bone marrow mesenchymal stem cells (rBMSCs) laden bioink for the ex-situ delivery approach as alternative delivery strategies. We found that in-situ delivery of PEI-pBMP-2 significantly improved bone tissue formation compared to ex-situ delivery. Despite debates amongst individual advantages and disadvantages of ex-situ and in-situ delivery strategies, our results ruled in favor of the in-situ delivery strategy, which could be desirable to use for future clinical applications.

Keywords

In-situ delivery; ex-situ delivery; gene therapy; stem cells; bone tissue engineering; intraoperative bioprinting

1. Introduction

Non-viral gene delivery based therapeutics for bone regeneration, including the delivery of foreign nucleic acids or osteogenic genes into cell milieu, has gained significant attention in inducing osteogenesis *in vivo* leading to accelerated bone repair [1, 2]. It is difficult for most non-viral gene vectors to pass through the plasma membrane on their own due to their negative surface charges and hydrophilicity [3, 4]. Therefore, researchers have used delivery vehicles, including polymers and liposomes, in order to form complexes to achieve stable carrier systems and sufficient transfection efficiency [4–6]. Polyethylenimine (PEI) is one of the most commonly used synthetic cationic polymer for efficient delivery of nucleic acids (encoded plasmid-DNA (pDNA)) into cell nuclei by the formation of PEI-pDNA polyplexes, also known as complexes or nanoplexes, through electrostatic interactions [7, 8]. The PEI-pDNA polyplex causes the endosome to swell and rupture due to osmolysis enabling earlier escape of complexes before lysosomal degradation; this is known as the proton sponge effect [7–9].

Both ex-situ [10, 11] and in-situ [12–14] delivery of pDNA into the targeted defect region have been previously investigated in order to test their efficiency in tissue repair and potential use in therapeutic applications [15]. The ex-situ delivery strategy involves transfection of specific cell population with a desirable gene outside of the body before *in vivo* delivery [2]. Therefore, this strategy provides direct targeting of cells to uptake the gene of interest during the transfection process resulting in pre-determined transfection efficiency before their use *in vivo* [16]. However, ex-situ delivery mechanism requires more processing time due to the cell culture work prior to transfection and implantation, which is not desirable for clinical applications. Additionally, the stem cell extraction process from patients requires invasive surgical procedures and could be burdensome for patients in critical conditions [10, 11, 15, 17]. On the other hand, in-situ delivery strategy of gene-based

growth factors could be a more attractive approach since it does not require cell extraction and expansion, and prolonged cell culture time are all avoided providing less complicated treatment for the repair of bone defects [18]. However, the in-situ delivery approach does not allow direct delivery of these polymer-based pDNA delivery vehicles into the specific cell population *in vivo*, causing possible side-effects due to non-specific interactions and uptake of the complexes by non-targeted cells [11, 15, 17].

In this study, we evaluated both ex-situ and in-situ delivery of PEI-pBMP-2 and compared their potential in repairing critical-sized rat calvarial bone defects using the intraoperative bioprinting (IOB, which is also known as in-situ or in-vivo bioprinting [19]) as a tool as highlighted in Fig. 1. Here, an osteogenic hard tissue bioink, developed in a previous work [20], where PEI-plasmid bone morphogenetic protein-2 (PEI-pBMP-2) polyplexes were loaded in to the bioink as the in-situ delivery strategy. On the contrary, PEI-pBMP-2 polyplexes were used to transfect rat bone marrow mesenchymal stem cells (rBMSCs(tPEI-pBMP-2)) and then transfected cells were loaded into the bioink for IOB for the ex-situ delivery strategy. The IOB technology made it feasible to directly deliver gene-activated matrices in an anatomically customized shape into the calvarial defect site. Overall, this study aimed to compare in-situ and ex-situ delivery of PEI-pBMP-2, and the demonstrated results suggest the possibility of expanding the scope of gene delivery via IOB for bone regeneration.

2. Materials and Methods

2.1. pDNA Preparation

pDNAs were prepared based on a previously published study [21]. Briefly, the chemically competent DH5α™ bacterial strain (*Escherichia colispecies*) was transformed with pBMP-2 (cat. no. SC119392, Origene Technologies, Rockville, MD). The transformed cultures were then expanded in Lennox L Broth (Research Products Incorporated, MT. Prospect, IL) overnight at 37 °C in an incubator shaker at 300 RPM. pDNA was extracted using a GenElute™ HP endotoxin-free plasmid maxiprep kit (cat. no. NA0410–1KT, Sigma-Aldrich, St. Louis, MO) and analyzed for purity using a Zetasizer Nano-ZS (Malvern Instruments, Westborough, MA) by measuring the ratio of absorbance (A260 nm/A280 nm).

2.2. Formation of PEI-pDNA Polyplexes

PEI-pBMP-2 (N/P ratio of 10, where “N=molar number of primary amines in the polymer; P=molar number of phosphate groups in the pDNA backbone” [10]) complexes were formed by the addition of 75 μg of plasmid DNA (2000 μg/ml) into 100 μl of PEI (2 mg/ml) (Sigma-Aldrich, cat. no. 408727, MW: 25k) solution by manual pipetting [12] and further incubated at room temperature for 30 min. The use of N:P ratio 10 in the transfection of stem cells was based on extensive optimization studies carried out in earlier studies. These include studies comparing branched and linear PEI at different N:P ratios *in vivo* [22], showing that an N:P ratio of 10 is optimal for transfection efficacy in human bone marrow stromal cells [12], human embryonic palatal mesenchyme cells [23] and human adipose derived mesenchymal stem cells [24].

2.3. Characterization of PEI-pDNA Polyplexes

After the formation of PEI-pBMP-2 complexes, the particle size distribution, mean particle size, polydispersity index (PDI) and zeta potential measurements were investigated (in triplicates) using Malvern Zetasizer Nano ZS instrument (Worcestershire, UK) at 25 °C.

2.4. Bioink Preparation

The bioink was prepared according to a recent work [20]. Briefly, 56% (w/v) β-glycerophosphate (βGP, Sigma-Aldrich) combined with 2% (w/v) chitosan solution (CS, Sigma-Aldrich, cat. no. 417963h) at a volumetric ratio of 1:9 (v/v) (βGP:CS). Type-I collagen extracted from rat tails [25] was dissolved in 0.02N acetic acid solution at a concentration of 9 mg/ml (Coll) and then mixed with neutralized CS-βGP solution at a ratio of 1:4 (v/v) (Coll:CS-βGP). Next, freeze-dried collagen sponges were added to the solution to prepare a final concentration of 26.6 mg/ml of collagen and mixed for 30 min using an in-house developed paste mixer at room temperature until a homogenous solution was achieved. Finally, nano-hydroxyapatite particles (nHAp) (nanoXIM-HAp202, Fluidinova, Portugal) were added to the overall bioink solution and mixed for additional 10 to 15 min to achieve 106.67 mg nHAp/ml.

2.5. Bioink Preparation for in-situ Delivery

A total of 1250 μg of pBMP-2 was complexed with PEI (Sigma-Aldrich) to form polyplexes to deliver 50 μg of PEI-pBMP-2 complex per defect *in vivo* (25 constructs per batch). The freeze dried polyplexes were mixed with the bioink solution using the in-house paste mixer until a homogenous mixture was achieved.

2.6. Cell Culture

For in-vitro study, human mesenchymal stem cells (hMSCs, RoosterBio Inc., MD, USA) were cultured using MSC expansion media (R&D Systems, MN, USA) (growth media; GM) supplemented with Penicillin (100 IU/ml) - Streptomycin (100 μg/ml) (cat. no. 30–002-CI, Corning Life Sciences, Lowell, MA) until usage. As an osteogenic media (OM), human osteogenic differentiation media (Cell Applications, USA) added with Penicillin-Streptomycin was used.

For in-vivo study, as implantation of hMSCs was not possible into immunocompetent rats, allogenic rBMSCs were extracted from inbred 4-week-old male Fischer white rats (F344/DuCrl, Charles River Laboratories, Wilmington, MA) [25]. All animals were cared in the animal facility (Millennium Science Complex, PSU) and euthanasia procedures were according to American Association for Laboratory Animal Science (AALAS) and The Institutional Animal Care and Use Committee (IACUC protocol #46591). Isolated rBMSCs were plated on 6-well cell culture plates in Minimal Eagle's Medium, Alpha modification (αMEM; cat. no. 10–022-CV, Corning Cellgro®, Manassas, VA) supplemented with 10% fetal bovine serum (FBS) (cat. no. 35–010-cv, Thermo Fisher Scientific, Waltham, WA), PS and 2.5 μg/ml Fungizone (cat. no. 15–290-026, Thermo Fisher Scientific) and incubated at 37 °C in a humidified 5% CO_2 incubator.

2.7. Bioink Preparation for Ex-Situ Delivery

Ex-situ delivery method was accomplished with transfecting hMSCs or isolated rBMSCs with PEI-pBMP-2 complexes, for in-vitro and in-vivo studies, respectively. rBSMCs at 0.5 million were transfected for one reaction of PEI-pBMP-2 complex (75 μg pDNA/100 μl of PEI complex). The PEI complex dropwise was pipetted onto 2D seeded hMSCs or rBMSCs in αMEM (serum-free media) and mixed gently to ensure homogenous distribution over the cell growth area. The cells were then incubated at 37 °C for 4 h and then replaced with growth medium containing serum according to a previously published study [26]. The following day, 5 million hMSCs or rBMSCs (tPEI-pBMP-2) were collected and mixed with 1 mL of bioink. ~320,000 transfected rBMSCs were loaded per construct and 50 μg of PEI-pBMP-2 was used per defect.

2.8. 3D Bioprinting of constructs for the in-vitro study

The in-house developed Multi-Arm BioPrinter (MABP) [27] was used for 3D bioprinting samples for the in-vitro study. The constructs were 3D bioprinted (using transfected or non-transfected hMSCs at 5 million cells/mL loaded into the bioink) at a bioprinting speed of 60 mm/min, a nozzle diameter of 410 μm and pneumatic pressure of 80 kPa. Bioprinting was performed at room temperature (25 °C) and the bioink was deposited on a temperature-controlled plate set at 44 °C [25]. The constructs were bioprinted in 5-mm diameter and 1-mm thickness, like the defect shape. Then, constructs loaded with transfected and non-transfected hMSCs were cultured with OM and GM, respectively. During the culture period, media was changed every other day.

As a negative control group, two-dimensional (2D) cultures were fabricated. For morphological characterization, 160,000 hMSCs were seeded on 22 mm × 22 mm sterile glass slides, which were placed inside a 6-well plate for culture. For quantitative real-time polymerase chain reaction (RT-PCR) test, 320,000 hMSCs were seeded on 6-well plates, and GM or OM were added thereafter for transfected and non-transfected hMSCs, respectively.

Next, in-vitro study was proceeded using four groups: i) 2D hMSCs transfected with PEI-pBMP-2 and cultured in GM, ii) 2D hMSCs cultured in OM, iii) 3D bioprinted hMSCs transfected with PEI-pBMP-2 and cultured in GM, and iv) 3D bioprinted hMSCs cultured in OM.

2.9. Cell Viability

To measure cell viability, LIVE/DEAD staining was performed using Calcein (0.15 mM) and ethidium homodimer-1 (2 mM) at Days 1 and 7. 2D and 3D bioprinted samples were stained for 30 min and captured using a Zeiss Axio Zoom fluorescent microscope (Carl Zeiss, Germany). Cell viability was obtained by the percentage of the number of live cells to the total number of cells.

2.10. Immunofluorescence staining

Cell morphology and osteogenic differentiation were observed by immunofluorescence staining at Days 7 and 21. To begin, 2D and 3D samples were fixed using 4% paraformaldehyde for 12 h at 4 °C. The following day, the samples were treated with

0.3% Triton X-100 for 15 min and 10% normal goat serum (NGS) for 2 h. A mouse anti-runt-related transcription factor (RUNX2) antibody (1:500; ab76956, Abcam) and rabbit anti-bone sialoprotein (BSP; 1:500; ab52128, Abcam) were used to conjugate antibodies with samples at 4 °C for a day. After rinsing the samples using Dulbecco's phosphate-buffered saline (DPBS) once, nuclei and F-actin were stained by Hoechst (1:500; blue; Life Technologies) and phalloidin (1:100; red; a12380, Molecular Probes); osteogenic differentiation of hMSCs was visualized using Alexa Fluor 488 goat anti-mouse IgG (H+L) secondary antibody (1:250; green; A11017, Invitrogen) and Alexa Fluor 647 goat anti-rabbit IgG (H+L) secondary antibody (1:250; cyan; A21245, Invitrogen). The samples were immersed in a staining solution for 1.5 h in an incubator at 37 °C before imaging using a Zeiss LSM880 confocal microscope (Carl Zeiss, Germany).

2.11. Reverse transcription polymerase chain reaction (RT-PCR)

For a quantitative measurement, gene expression was analyzed by RT-PCR. Both 2D and 3D samples were prepared and cultured for 28 d. TRIzol® reagent (Thermo Fisher Scientific) was used to isolate RNA from the samples, in which its concentration was measured by reading the absorbance to obtain the ratio of 260/280 nm using a NanoDrop (ND-1000 Spectrophotometer, Thermo Fisher Scientific). Complementary deoxyribonucleic acid (cDNA) synthesis was carried out using T100 Thermal Cycler (BioRad) according to the manufacturer's protocol of AccuPower® CycleScript RT PreMix (Bioneer, Korea). Thereafter, gene expression was analyzed with SYBR Green (Thermo Fisher Scientific) using a StepOnePlus Real-Time PCR System (Applied Biosystems). Each gene was filled in a 96-well plate. The fold-change of genes, including Col1, RUNX2, OCN, and BSP, was calculated using the $2^{-\Delta\Delta CT}$ method and normalized with respect to housekeeping gene, glyceraldehyde 3-phosphate dehydrogenase (GAPDH). Then, all groups were normalized to hMSCs at Day 1, which were set as 1-fold. The reader is referred to Table for a list of primers used in RT-PCR.

2.12. Surgical Procedures for Intraoperative Bioprinting

A total of 11 12-week-old inbred male Fischer 344 white rats were anesthetized with an intraperitoneal injection of ketamine (Midwest Veterinary, Lakeville, MN) mixed with xylazine (LLOYD Inc., Shenandoah, IA) at a dose of 100 mg/kg for ketamine and 10 mg/kg for xylazine after inhalation of isoflurane (2–5%) over 1–2 mins. When animals were fully anesthetized, artificial tears (Rugby Laboratories, Livonia, MI) were placed on eyes, and heads were shaved and treated with a betadine surgical scrub followed by ethanol. Bupivacaine (0.015 mg/kg) (Centralized Biological Laboratory, PSU) at a concentration of 2.5 mg/mL and buprenorphine (0.015 mg/kg) were injected subcutaneously before the surgery. A sagittal incision was made through the periosteum and was retracted to expose the calvarium. Two critical-sized calvarial defects (each with 5 mm in diameter) were drilled into the parietal bone on each side of the rat skull using a trephine bit, keeping the Dura mater intact.

The experiment was designed to include four major groups: i) negative control (n=3), ii) bioink+rBMSCs (5 million cells/ml) (n=6), iii) bioink+rBMSCs(tPEI-pBMP-2) (n=6) for ex-situ delivery, and iv) bioink+PEI-pBMP-2 (n=7) for in-situ delivery of plasmid particles.

IOB was performed by pneumatically extruding the bioink using the in-house developed MABP [27] system following a spiral deposition at a bioprinting speed of 60 mm/min. Thereafter, periosteum and skin were sutured with simple interrupted 5–0 monocryl (Ethicon Inc., Somerville, NJ) and 4–0 vicryl (Ethicon Inc.) sutures, respectively. After the surgeries, animals were placed on warming pad allowing recovery and were observed closely until they awoke from sternal recumbency. Following the post-surgery recovery, a single dose of buprenorphine was administered every 12 h for a minimum of 24 h of analgesia. Animals were observed and weighed daily for at least 10 days post-surgery and weighed once a week after removing the sutures (10 days after the surgery). Animals were euthanized at 6 weeks post-surgery by CO_2 inhalation (2 L/min) until breathing cessation and subsequently decapitated.

2.13. Assessment of Bone Formation

Micro-computed tomography (μCT) scanning of calvarial defects was performed with a vivaCT 40 scanner (Scanco Medical, Switzerland) (17.5 μm isometric voxels, 70 kV energy, 114 μA intensity, and 200 ms integration time) [28]. Image analysis was conducted using a cylindrical 3D oriented volume of interest with a radius of 2.5 mm and a height of 1 mm in Avizo (FEI Company, Hillsboro, OR), MATLAB (Natick, MA) after applying a gaussian smoothing filter (sigma 0.9) and a threshold cutoff of 300 mgHA/cm^3. The bone volume divided by total volume (BV/TV%), normalized bone mineral density (BMD%) and bone coverage area (%) were calculated from the filtered and processed data. Note that, the volume fraction of nHAp in the bioink was calculated prior to in-vivo studies in order to determine the baseline mineralization and eliminate possible artifacts in the scanned samples from our calculations, which turned out to be negligibly small.

2.14. Histological Analysis

Calvarial explants were extracted from rat skulls at Week 6 post surgery, rinsed with DPBS and fixed with 4% paraformaldehyde for 2 days at 4 °C. The explants were then decalcified with 0.5M ethylenediaminetetraacetic acid (EDTA) disodium salt (Research Products International, Mount Prospect, IL) for 6 weeks at 4 °C. After the decalcification process, samples were embedded in O.C.T. cyromatrix (Thermo Fisher Scientific) embedding resin, sectioned using a Leica CM1950 Cryostat (Leica Biosystems, Wetzlar, Germany) at −32 °C with 18 μm thickness, and stained in a Hematoxylin and Eosin (H&E) automated staining platform (Leica Auto Stainer XL, Leica Biosystems) without applying any heat during the staining process. The stained sections were mounted using Neo-Mount® anhydrous mounting medium (Millipore) and imaged using a Keyence BZ-9000 (Keyence Corporation of America, Elmwood Park, NJ) fluorescence microscope under the bright field using a neutral density optical filter.

In order to visualize the collagen deposition histomorphometrically, sectioned samples were also stained using Masson's Trichrome staining (MTS) kit (Sigma-Aldrich, cat. No. HT15–1KT) based on the manufacturer's instructions. The stained samples were dehydrated gradually with ethanol, using Neo-Mount® anhydrous mounting medium (Millipore), and imaged using the Keyence BZ-9000 microscope as described before.

2.15. Statistical Analysis

All data were presented as mean ± standard deviation unless stated otherwise. In order to compare three or more groups, data were analyzed by one-way ANOVA with post hoc Fisher's individual tests for differences of means at a 95% confidence level (assuming equal variances). Differences were considered significant at $p^{***}<0.001$, $p^{**}<0.01$, $p^{*}<0.05$. All statistical analysis was performed using Minitab 17.3 (Minitab Inc., State College, PA).

3. Results

The average size of the PEI-pBMP-2 polyplexes used in this study was determined to be 1.4 μm. These polyplexes had the potential to be taken up by cells through the macropinocytosis pathway allowing the entry of micron-sized particles through large vesicles (0.5 – 10 μm) present on the plasma membrane [29]. A PDI value of ~0.66 indicated a large diversity in size distribution amongst the PEI-pBMP-2 polyplexes, which might affect the transfection efficiency of the polyplexes (Fig. 2A). The zeta potential was measured as 25mV demonstrating positively charged particles (Fig. 2B).

Cytocompatibility of the transfection (using PEI-pBMP-2) and 3D bioprinting processes was evaluated via LIVE/DEAD assay (Fig. 3A). For in-vitro evaluation, hMSCs were used at a density of 5 million cells/mL in the bioink. Specifically, four groups were used including i) 2D transfected hMSCs cultured in GM (2D-T), ii) 2D hMSCs treated with osteogenic media (OM) (2D-OM), iii) 3D bioprinted constructs loaded with transfected hMSCs and treated with GM (3D-T), and iv) 3D bioprinted constructs loaded with hMSCs and treated with OM (3D-OM). Each group was analyzed for cell viability at Days 1 and 7 (Fig. 3B). All groups showed high cell viability (> 90%), which was maintained from Day 1 through 7, highlighting the fact that the transfection and bioprinting processes did not impair the viability of hMSCs.

For the same experimental groups, morphology and osteogenic differentiation of hMSCs were confirmed by immunofluorescent images showing phalloidin, RUNX2, and BSP counterstained with Hoechst (Fig. 4A). To elaborate, RUNX2, a multifunctional transcription factor for osteogenesis, was expressed in the nucleoplasm for all groups at Day 7 and became more evident at Day 21 (Fig. 4A). Whereas BSP, a marker expressed at the late stage of ostegenesis, was not expressed in 2D groups at Day 21, but 3D groups revealed BSP expression at Day 21 (Fig. 4A). These results suggest that 3D bioprinted constructs and PEI-pBMP-2 transfection facilitated the osteogenic differentiation of hMSCs.

Furthermore, the expression of osteogenic markers (RUNX2, Col1, OCN, and BSP) were evaluated using RT-PCR. RUNX2 was 75-, 61-, and 14-fold higher on 3D-T compared to 2D-T, 2D-OM, and 3D-OM, respectively. For Col1, an early-stage osteogenic marker, 3D-T and 3D-OM revealed significantly higher expression compared to 2D-T and 2D-OM. On the other hand, although OCN, a marker of mature osteoblasts, did not show any significant difference among all groups, 3D-T and 3D-OM were ~72- and ~28-fold higher compared to 2D groups, respectively. In the meantime, BSP, which can be found specific for mineralized tissues, was significantly expressed in both 3D groups.

After confirming the cytocompatibility of the process and the osteogenic potential of the pBMP-2-transfected hMSC-laden 3D bioprinted constructs *in vitro*, IOB process was performed using MABP after surgically opening two, 5 mm-diameter critical-sized calvarial defects on rat skulls (Fig. 5), which is a well-established model for bone repair in the literature as a size of one tenth of skull does not heal spontaneously during the lifetime [30]. The animal head position was maintained fixed during surgeries. Next, IOB was performed by directly bioprinting bone constructs onto the defect site(s) allowing printhead to follow a spiral toolpath plan with a 100% infilled density to ensure complete filling of each defect in a controlled manner, where overall IOB process took <1 min per construct. In this study, we employed four groups including i) empty defect (control), ii) rBMSCs-laden bioink (no delivery), iii) rBMSCs(tPEI-pBMP-2)-laden bioink (ex-situ delivery), and iv) PEI-pBMP-2-laden bioink (in-situ delivery). The bioink crosslinking after extrusion was achieved by temperature induced physical crosslinking of collagen and CS-βGP at body temperature resulting in a rapid solution to gelation phase transition [31].

Six weeks post bioprinting, rats were euthanized for the evaluation of bone regeneration. Overall, both newly formed bone tissue and mineralized bone matrix were observed in all groups via μCT scanning (Fig. 6A). The in-situ delivery group demonstrated significant improvement in bone volume to total bone volume percentage (BV/TV) (%) compared to empty (~1.94-fold, $p<0.001$), no delivery (~1.86-fold, $p<0.001$) and ex-situ delivery (~1.33-fold, $p=0.012$) groups (Fig. 6B1). Additionally, the ex-situ delivery group improved bone repair significantly compared to the no delivery (~1.4-fold, $p=0.030$) and empty (~1.46-fold, $p=0.048$) groups. The normalized percentage bone mineral density (BMD) was determined to be higher for the in-situ delivery group compared to the empty (~1.8-fold, $p<0.001$), no delivery (~1.4-fold, $p<0.001$) and ex-situ delivery (~1.2-fold, $p=0.030$) groups, respectively (Fig. 6B2). Additionally, the ex-situ delivery group showed ~1.6-fold ($p<0.001$) increase in normalized BMD% compared to the empty group and no significant difference was observed compared to the no delivery group. The no delivery group, on the other hand, demonstrated higher normalized BMD% compared to the empty group (~1.32-fold, $p=0.045$). No significant difference was observed between ex-situ and in-situ delivery of pDNAs in terms of the bone coverage area. In-situ and ex-situ delivery groups demonstrated ~1.8- ($p<0.001$) and 1.7-fold ($p=0001$) increase in bone coverage area compared to the empty group, respectively (Fig. 6B3). The in-situ delivery group also showed a 1.3-fold-increase in bone coverage area compared to the no delivery group ($p=0.009$), whereas no significant difference ($p=0.057$) was observed for the ex-situ delivery group. The no delivery group showed higher bone coverage area (~1.4-fold, $p=0.048$) in comparison to that of the empty defect.

Hematoxylin and eosin (H&E) staining and Masson's Trichrome staining (MTS) were performed on the decalcified sections to visualize the newly formed bone tissue matrix histomorphometrically. H&E images demonstrated the connectivity and compactness of newly formed bone tissue in the calvarial defects. The empty group demonstrated mostly soft tissue (ST) formation, which was visualized with a lightly pink color. A partial amount of newly regenerated bone tissue (RB) was detected nearby the defect edges in the empty group (Fig. 7A1). While the remaining groups were able to form bony bridge invading from one defect edge to another (Figs. 7A2–A4). The no delivery group had less dense RB tissue

compared to ex-situ and in-situ delivery groups (Fig. 7A2). The highest nuclei density was also observed in the in-situ delivery group, which displayed densest RB tissue area with the least amount of ST formation compared to the other groups (Fig. 7A4).

The MTS images were used to display collagen matrix with bluish areas indicating immature and mature bone tissues in the calvarial bone defects (Figs. 7A1–4). The mature bone stained with a dark blue color, whereas the fibrous tissue with lightly blue color. The empty group demonstrated mainly light blue color and immature bone formation near by the host bone (HB), which were taken a dark blue color (Fig. 8A1). Additionally, there were quite many apparent red blood cells in the defect site indicating vascularization during ongoing bone repair process. Both no delivery (Fig. 8A2) and ex-situ delivery (Fig. 8A3) groups exhibited a dense blue color nearby HB compared to the empty group. The in-situ delivery group had noticeable dense blue islands indicating immature bone formation throughout the defect (Fig. 8A4).

4. Discussion

In this study, the concept of combining the delivery of PEI complexed pDNA encoding BMP-2 with IOB was demonstrated for craniomaxillofacial (CMF) bone regeneration. The attempts on delivery or transfection using various micro/nanoparticles, such as microRNA, chemically modified RNA, and cytokines, have been demonstrated to manipulate cell fate [28, 32, 33], but direct delivery via IOB is still in its infancy.

To prove this concept, we began with an in-vitro study to show the effect of PEI-pBMP-2 and bioprinting on cellular activities including cell viability and osteogenic differentiation. As a control, hMSCs with and without transfection were cultured in 2D. Here, high cell viability (>90%) was observed at Days 1 and 7 regardless of transfection indicating that the transfection using PEI-pBMP-2 did not impair cell viability. Then, non-transfected and transfected hMSCs were used to bioprint 3D hMSC-laden constructs to compare the fate of hMSCs with respect to those in 2D groups. Similarly, 3D groups showed high cell viability (>90%) up to Day 7, which demonstrated the feasibility of bioprinting of PEI-pBMP-2-transfected progenitors for bone tissue engineering applications.

In addition, the effect of PEI-pBMP-2 on the osteogenic differentiation of hMSCs was compared to that of the osteogenic media. The immunofluorescent images demonstrated that the expression of RUNX2 became more evident from Day 7 to 21 in both 2D and 3D groups. However, BSP was present only in 3D groups, which might be due to the synergistic effects of PEI-pBMP-2 transfection and presence of collagen in the 3D microenvironment [27, 33, 34]. For instance, rat BMSCs embedded in a methacrylamide gelatin bioink with BMP-2-collagen microfibers showed greater expression of osteogenic markers (alkaline phosphatase (ALP), BSP, OCN, and Col1) compared to those cultured without BMP-2-collagen microfibers [33]. To elaborate, BMP-2 and collagen have shown supporting effects in cell adhesion, migration, and differentiation, and for some clinical trials, eventually guided successful interbody fusions [35–37]. Hence, these results denote that the combinatorial approach of delivering PEI-pBMP-2 and the osteogenic bioink was favorable for osteogenesis.

The degree of osteogenesis was further examined quantitatively by RT-PCR. The results reveal that the transfected groups were as effective as OM groups to induce osteogenesis in both 2D and 3D environment. Compared with 2D groups, 3D groups generally showed higher quantitative values, which suggest that bioprinting is advantageous by providing a 3D microenvironment for progenitors to differentiate osteogenically. Since one of the purposes of IOB was to minimize the pre-processing time (i.e., cell preparation or culture period), transfected cells (ex-situ delivery) or in-situ delivery of PEI-pBMP-2 can be an efficient approach to induce osteogenesis when directly bioprinted into a defect site without differentiating cells for a long culture period prior to bioprinting.

In order to test the effectiveness of PEI-pBMP-2 using in-situ versus ex-situ delivery, we utilized IOB, which is deemed an effective technology for direct deposition of constructs into the defect site. This technology was previously demonstrated for the repair of calvarial bone defects in a mouse model using a laser-assisted bioprinting (LAB) system by delivering hydroxyapatite in collagen [34]. Even though LAB has a higher resolution, it might not be ideal for use in IOB towards translating this technology into clinics due to its time-consuming nature and operational complexity [35]. Thus, extrusion-based bioprinting would be more suitable to directly print viscous bioinks into a defect site for hard tissue repair owing to its ease with scalability, and the ability to bioprint constructs in a simpler and rapid manner [36]. Although manual injection can also be utilized to deliver the bioink into the defect, IOB enables avoiding inconsistent deposition and non-uniform extrusion of bioink that eventually alters the amount of PEI-pDNA affecting cellular activities. In addition, to reconstruct complex-shaped contour zones of the cranium, IOB is a great tool providing a degree of freedom by its high precision and versatility, which can be utilized for high precision applications, such as IOB of thinner tissues (i.e., skin) or combination of such thinner tissues with the bone as demonstrated recently [20].

This study is the first attempt investigating the efficacy of in-situ versus ex-situ delivery of bioprinted PEI-pBMP-2 polyplexes to determine the more efficient delivery method for the repair of rat critical size calvarial defects. To improve the functionality of stem cells delivered to the defect site, there is a growing evidence that the delivery of gene-based growth factors within the cell membrane can be beneficial for improved vascularization [26] and mineralized bone tissue formation [37]. One of the greatest advantages of ex-situ delivery mechanism is to target a specific cell population and load it into the bioink before the delivery of gene activated matrices *in vivo*. In our study, ex-vivo transfection of rBMSCs were achieved in a 2D culture and then transfected cells were loaded into the bioink before the in-vivo delivery. This way, we could assume that the delivered stem cells had the ability to commit to osteogenic differentiation producing desired bone matrix proteins *in vivo* [17]. To the best of our knowledge, there has been no study demonstrating implantation of constructs *in vivo* using an ex-situ delivery method, specifically using stem cells that are transfected with PEI-based gene carriers for osteogenesis inducing factors. It has been previously reported that PEI-pDNA polyplexes transfected rBMSCs (1μg pDNA per 3×10^4 cells) resulted in around 2–10% of transfection efficiency depending on N/P ratios [38]. In this study, we observed that transfection of rBMSCs with PEI-pBMP-2 polyplexes improved bone regeneration significantly compared to non-transfected rBMSCs despite its potentially low transfection efficiency in a 2D culture. On the other hand, the delivery of transfected

rBMSCs into the defect site via IOB can also witness other challenges. For example, one of the major clinical concerns for injured CMF defects is the disruption of blood vessels surrounding the exposed defect site resulting in insufficient bone repair due to lack of vascular network formation, which eventually causes osteonecrosis [39]. Bone regeneration and repair depends on an effective vascular network of blood vessels to transport waste, nutrients, and other essential molecules [40]. After the delivery of cells into the defect site via IOB, damaged blood vessels surrounding the periphery of the defect might not have enough support of oxygen and nutrients to sustain the viability of cells and support their growth until newer blood vessels were formed. This could potentially lead to necrosis after the delivery of cells into the defect side due to hypoxia and starvation [41]. Therefore, vascularization will become a critical factor for the repair of larger CMF defects and the preservation of the viability of delivered cells *in vivo*. In this regard, incorporation of angiogenic pDNA encoding growth factors, such as vascular endothelial growth factor, fibroblast growth factor or platelet-derived growth factor, can mediate vasculogenic response to enhance vascularization during the bone remodeling process [42]. Additionally, the incorporation of oxygen releasing micro-particles can be considered, which will enable oxygenization of cells until vascularization takes place [43, 44].

In this study, we used 5×10^6 rBMSCs per mL, where the cell encapsulation density for hydrogels has been varied from 5 to 10 million cells/ml for bone tissue engineering [45]. On the other hand, the delivery of high cell density within the bioink might prove to be yet another reason for reduced bone formation. It has been previously shown that cell-to-cell distance effects osteogenic gene expression during osteogenesis [46]. Increased osteogenic gene markers, including ALP, OCN, Col1 and RUNX2, was noted on Days 8 and 14 when the seeding density of human umbilical cord mesenchymal stem cells on calcium-phosphate cement was 300k compared to 50k [47]. On the contrary, reduced osteogenic activities and mineralization was reported on Day 14 when the cell density was 500k instead of 300k [47]. In addition to the required optimal cell density, the localization of cells (for example, near periosteum) on bone grafts also acts as yet another important factor to allow easier access to oxygen and nutrient source for cells [48]. In calvarial defects, the areas which are rich in blood vessels are the periphery of defect sites and periosteum. Therefore, bioprinting cells on top of bone grafts (along with cell encapsulation) might improve bone formation *in vivo*. In a nutshell, the potential reasons for lesser newly formed bone tissue for the bioink+rBMSCs (no delivery) group might be associated with two reasons: i) degradation of the bioink due to the growing number of rBMSCs inside, and ii) rBMSCs are not committed osteogenically due to limited osteogenic ques (such as BMP-2); rather, they grow and proliferate more. In this regard, as bone damage gets more extensive, multipotent nature of rBMSCs can be a potential risk like developing granulated tissues unless an undesired lineage progression can be completely avoided and controlled [49]. Moreover, the usage of allogenic BMSCs is not yet a fully validated method due to possibility of inflammation and immune rejection [50]. For these reasons, the transplantation of BMSCs can generate unexpected or impaired in-vivo results.

Despite several disadvantages including the possibility of unknown uptake of pDNAs from a wide variety of cell types or non-specific cell targeting *in vivo* [15], or the attachment of released pDNA to HAp particles forming larger complexes resulting in lower uptake

of PEI-pBMP-2 complexes by cells [51], the in-situ delivery of PEI-pBMP-2 resulted in significant improvement in bone tissue repair and formation of mineralized bone tissue compared to the ex-situ delivery group. The potential reasons for the in-situ delivery strategy inducing improved bone regeneration could be due to the acellular form of the bioprinted constructs resulting in slower degradation [20] and sustained release of the PEI-pBMP-2 polyplexes compared to the cellular constructs. In specific, the addition of cells into the bioink (ex-situ or no delivery) could cause reduced bone formation by a series of effects such as reduced hydrogel stiffness leading to accelerated degradation rate and physical instability of bioprinted constructs. For instance, among collagen constructs seeded with 6×10^5, 3×10^6, 3×10^7, and 1×10^8 cells/mL, a scaffold with cell density above 3×10^6 cells/mL revealed a significant decrease in break force when tensile testing was performed immediately after compression at Day 10 [52]. Further, cell-induced collagenase activity expressed by matrix metallopeptidase 1 could be another factor resulting in a rapid breakdown of collagen matrix [52]. Hence, owing to the improved physical stability of bioprinted acellular constructs enabling the delivery of PEI-pDNA, we can conclude that the in-situ delivery provided a more favorable microenvironment for bone formation.

5. Conclusion

In this study, we investigated the repair capability of ex-situ and in-situ delivery strategies for bone therapeutic applications. The gene-activated matrices were loaded into a collagen-based bioink and delivered into critical-sized calvarial defects using the IOB technology, which enabled direct bioink deposition into calvarial defects via an extrusion-based system. The delivery of PEI-pBMP-2 loaded bioink resulted in higher bone regeneration compared to the ex-situ delivery and no delivery groups. Overall, the in-situ delivery of gene-based growth factors combined with IOB technology could be beneficial to promote accelerated bone repair, which could be an effective and practical strategy.

Acknowledgements

This work was supported by the National Institute of Dental and Craniofacial Research Award # R01DE028614 (I.T.O.), National Science Foundation Award #1600118 (I.T.O.), Osteology Foundation Award # 15–042 (I.T.O.) and International Team for Implantology Award # 1275_2017 (I.T.O.). The authors are also grateful to R&D Systems for the generous support. The authors would like to thank Dante Deluca for his contributions to cryosectioning of calvarial explants, Kevin Godzik for his assistance to with the preparation of the bioink, and Dishary Banerjee for her assistance with preparing and transfecting cells. The authors are also thankful to The Huck Institute of The Life Sciences at PSU for the generous facility support.

Data availability statement

All data that support the findings of this study are included within the article.

References

[1]. Betz VM, Betz OB, Harris MB, Vrahas MS and Evans CH 2008 Bone tissue engineering and repair by gene therapy Front. Bioscience-Landmark 13 833–41

[2]. Evans C 2011 Gene therapy for the regeneration of bone Injury 42 599–604 [PubMed: 21489526]

[3]. Khalil IA, Kogure K, Akita H and Harashima H 2006 Uptake pathways and subsequent intracellular trafficking in nonviral gene delivery Pharmacological rev 58 32–45

[4]. Cohen H, Levy R, Gao J, Fishbein I, Kousaev V, Sosnowski S, Slomkowski S and Golomb G 2000 Sustained delivery and expression of DNA encapsulated in polymeric nanoparticles Gene Ther 7 1896–905 [PubMed: 11127577]

[5]. Csaba N, Sanchez A and Alonso MJ 2006 PLGA: poloxamer and PLGA: poloxamine blend nanostructures as carriers for nasal gene delivery J. Controlled Release 113 164–72

[6]. Bhakta G, Mitra S and Maitra A 2005 DNA encapsulated magnesium and manganous phosphate nanoparticles: potential non-viral vectors for gene delivery Biomaterials 26 2157–63 [PubMed: 15576191]

[7]. Densmore CL, Orson FM, Xu B, Kinsey BM, Waldrep JC, Hua P, Bhogal B and Knight V 2000 Aerosol delivery of robust polyethyleneimine–DNA complexes for gene therapy and genetic immunization Mol. Ther 1 180–8 [PubMed: 10933929]

[8]. Liang W and Lam JK 2012 Endosomal escape pathways for non-viral nucleic acid delivery systems Mol. Regul. Endocytosis 429–56

[9]. Zhao Q-Q, Chen J-L, Lv T-F, He C-X, Tang G-P, Liang W-Q, Tabata Y and Gao J-Q 2009 N/P ratio significantly influences the transfection efficiency and cytotoxicity of a polyethylenimine/chitosan/DNA complex Biol. Pharm. Bull 32 706–10 [PubMed: 19336909]

[10]. L Santos J, Pandita D, Rodrigues J, P Pego A, L Granja P and Tomás H 2011 Non-viral gene delivery to mesenchymal stem cells: methods, strategies and application in bone tissue engineering and regeneration Curr. Gene Ther 11 46–57 [PubMed: 21182464]

[11]. Blum JS, Barry MA, Mikos AG and Jansen JA 2003 In vivo evaluation of gene therapy vectors in ex vivo-derived marrow stromal cells for bone regeneration in a rat critical-size calvarial defect model Hum. Gene Ther 14 1689–701 [PubMed: 14670121]

[12]. Elangovan S, D'Mello SR, Hong L, Ross RD, Allamargot C, Dawson DV, Stanford CM, Johnson GK, Sumner DR and Salem AK 2014 The enhancement of bone regeneration by gene activated matrix encoding for platelet derived growth factor Biomaterials 35 737–47 [PubMed: 24161167]

[13]. Curtin CM, Tierney EG, McSorley K, Cryan SA, Duffy GP and O'Brien FJ 2015 Combinatorial gene therapy accelerates bone regeneration: non-viral dual delivery of VEGF and BMP2 in a collagen-nanohydroxyapatite scaffold Adv. Healthcare Mater 4 223–7

[14]. Plonka AB, Khorsand B, Yu N, Sugai JV, Salem AK, Giannobile WV and Elangovan S 2017 Effect of sustained PDGF nonviral gene delivery on repair of tooth-supporting bone defects Gene Ther 24 31–9 [PubMed: 27824330]

[15]. D'Mello S, Atluri K, Geary SM, Hong L, Elangovan S and Salem AK 2017 Bone regeneration using gene-activated matrices AAPS J 19 43–53 [PubMed: 27655418]

[16]. Bleich NK, Kallai I, Lieberman JR, Schwarz EM, Pelled G and Gazit D 2012 Gene therapy approaches to regenerating bone Adv. Drug Delivery Rev 64 1320–30

[17]. Paidikondala M, Kadekar S and Varghese OP 2018 Innovative strategy for 3D transfection of primary human stem cells with BMP-2 expressing plasmid DNA: A clinically translatable strategy for ex vivo gene therapy Int. J. Mol. Sci 20 56 [PubMed: 30583610]

[18]. Evans C 2012 Gene delivery to bone Adv. Drug Delivery Rev 64 1331–40

[19]. Wu Y, Ravnic DJ and Ozbolat IT 2020 Intraoperative bioprinting: repairing tissues and organs in a surgical setting Trends Biotechnol 38 594–605 [PubMed: 32407688]

[20]. Moncal KK, Gudapati H, Godzik KP, Heo DN, Kang Y, Rizk E, Ravnic DJ, Wee H, Pepley DF and Ozbolat V 2021 Intra-operative bioprinting of hard, soft, and hard/soft composite tissues for craniomaxillofacial reconstruction Adv. Funct. Mater 2010858 [PubMed: 34421475]

[21]. Acri TM, Laird NZ, Geary SM, Salem AK and Shin K 2019 Effects of calcium concentration on nonviral gene delivery to bone marrow-derived stem cells J. Tissue Eng. Regener. Med 13 2256–65

[22]. Intra J and Salem AK 2008 Characterization of the transgene expression generated by branched and linear polyethylenimine-plasmid DNA nanoparticles in vitro and after intraperitoneal injection in vivo J. Controlled Release 130 129–38

[23]. D'Mello S, Salem AK, Hong L and Elangovan S 2016 Characterization and evaluation of the efficacy of cationic complex mediated plasmid DNA delivery in human embryonic palatal mesenchyme cells J. Tissue Eng. Regener. Med 10 927–37

[24]. Atluri K, Seabold D, Hong L, Elangovan S and Salem AK 2015 Nanoplex-mediated codelivery of fibroblast growth factor and bone morphogenetic protein genes promotes osteogenesis in human adipocyte-derived mesenchymal stem cells Mol. Pharmaceutics 12 3032–42

[25]. Moncal KK, Ozbolat V, Datta P, Heo DN and Ozbolat IT 2019 Thermally-controlled extrusion-based bioprinting of collagen J. Mater. Sci.: Mater. Med 30 1–14

[26]. Khorsand B, Nicholson N, Do A-V, Femino JE, Martin JA, Petersen E, Guetschow B, Fredericks DC and Salem AK 2017 Regeneration of bone using nanoplex delivery of FGF-2 and BMP-2 genes in diaphyseal long bone radial defects in a diabetic rabbit model J. Controlled Release 248 53–9

[27]. Ozbolat IT, Chen H and Yu Y 2014 Development of 'Multi-arm Bioprinter'for hybrid biofabrication of tissue engineering constructs Rob. Comput. Integr. Manuf 30 295–304

[28]. Moncal KK, Aydin RST, Abu-Laban M, Heo DN, Rizk E, Tucker SM, Lewis GS, Hayes D and Ozbolat IT 2019 Collagen-infilled 3D printed scaffolds loaded with miR-148b-transfected bone marrow stem cells improve calvarial bone regeneration in rats Mater. Sci. Eng. C 105 110128

[29]. Foroozandeh P and Aziz AA 2018 Insight into cellular uptake and intracellular trafficking of nanoparticles Nanoscale Res. Lett 13 1–12 [PubMed: 29299709]

[30]. Shang Q, Wang Z, Liu W, Shi Y, Cui L and Cao Y 2001 Tissue-engineered bone repair of sheep cranial defects with autologous bone marrow stromal cells J. Craniofacial Surg 12 586–93

[31]. Kim S, Nishimoto SK, Bumgardner JD, Haggard WO, Gaber MW and Yang Y 2010 A chitosan/β-glycerophosphate thermo-sensitive gel for the delivery of ellagic acid for the treatment of brain cancer Biomaterials 31 4157–66 [PubMed: 20185170]

[32]. Khorsand B, Elangovan S, Hong L, Dewerth A, Kormann MS and Salem AK 2017 A comparative study of the bone regenerative effect of chemically modified RNA encoding BMP-2 or BMP-9 AAPS J 19 438–46 [PubMed: 28074350]

[33]. Sun H, Wang J, Deng F, Liu Y, Zhuang X, Xu J and Li L 2016 Co−delivery and controlled release of stromal cell−derived factor−1α chemically conjugated on collagen scaffolds enhances bone morphogenetic protein−2−driven osteogenesis in rats Mol. Med. Rep 14 737–45 [PubMed: 27220358]

[34]. Keriquel V, Oliveira H, Rémy M, Ziane S, Delmond S, Rousseau B, Rey S, Catros S, Amédée J and Guillemot F 2017 In situ printing of mesenchymal stromal cells, by laser-assisted bioprinting, for in vivo bone regeneration applications Sci. Rep 7 1–10 [PubMed: 28127051]

[35]. Ozbolat IT, Moncal KK and Gudapati H 2017 Evaluation of bioprinter technologies Addit. Manuf 13 179–200

[36]. Datta P, Barui A, Wu Y, Ozbolat V, Moncal KK and Ozbolat IT 2018 Essential steps in bioprinting: From pre-to post-bioprinting Biotechnol. Adv 36 1481–504 [PubMed: 29909085]

[37]. Bayer EA, Fedorchak MV and Little SR 2016 The influence of platelet-derived growth factor and bone morphogenetic protein presentation on tubule organization by human umbilical vascular endothelial cells and human mesenchymal stem cells in coculture Tissue Eng. Part A 22 1296–304 [PubMed: 27650131]

[38]. Ahn HH, Lee MS, Cho MH, Shin YN, Lee JH, Kim KS, Kim MS, Khang G, Hwang KC and Lee IW 2008 DNA/PEI nano-particles for gene delivery of rat bone marrow stem cells Colloids Surf., A 313 116–20

[39]. Abdi SIH, Choi JY, Lau HC and Lim JO 2013 Controlled release of oxygen from PLGA-alginate layered matrix and its in vitro characterization on the viability of muscle cells under hypoxic environment Tissue Eng. Regener. Med 10 131–8

[40]. Holmes B, Bulusu K, Plesniak M and Zhang LG 2016 A synergistic approach to the design, fabrication and evaluation of 3D printed micro and nano featured scaffolds for vascularized bone tissue repair Nanotechnology 27 064001 [PubMed: 26758780]

[41]. Lee H-Y, Kim H-W, Lee JH and Oh SH 2015 Controlling oxygen release from hollow microparticles for prolonged cell survival under hypoxic environment Biomaterials 53 583–91 [PubMed: 25890754]

[42]. Yang Y-Q, Tan Y-Y, Wong R, Wenden A, Zhang L-K and Rabie ABM 2012 The role of vascular endothelial growth factor in ossification Int. J. Oral Sci 4 64–8 [PubMed: 22722639]

[43]. Willemen NG, Hassan S, Gurian M, Li J, Allijn IE, Shin SR and Leijten J 2021 Oxygen-releasing biomaterials: current challenges and future applications Trends Biotechnol 39 1144–59 [PubMed: 33602609]

[44]. Farris AL, Rindone AN and Grayson WL 2016 Oxygen delivering biomaterials for tissue engineering J. Mater. Chem. B 4 3422–32 [PubMed: 27453782]

[45]. Cidonio G, Glinka M, Dawson J and Oreffo R 2019 The cell in the ink: Improving biofabrication by printing stem cells for skeletal regenerative medicine Biomaterials 209 10–24 [PubMed: 31022557]

[46]. Ma J, Both SK, Yang F, Cui F-Z, Pan J, Meijer GJ, Jansen JA and van den Beucken JJ 2014 Concise review: cell-based strategies in bone tissue engineering and regenerative medicine Stem Cells Transl. Med 3 98–107 [PubMed: 24300556]

[47]. Zhou H, Weir MD and Xu HH 2011 Effect of cell seeding density on proliferation and osteodifferentiation of umbilical cord stem cells on calcium phosphate cement-fiber scaffold Tissue Eng. Part A 17 2603–13 [PubMed: 21745111]

[48]. Britannica E 2018 Available online: https://www.britannica.com/place Brazil (*accessed on* 27 March 2018)

[49]. Singer NG and Caplan AI 2011 Mesenchymal stem cells: mechanisms of inflammation Ann. Rev. Pathol.: Mech. Dis 6 457–78

[50]. Huang S, Xu L, Zhang Y, Sun Y and Li G 2015 Systemic and local administration of allogeneic bone marrow-derived mesenchymal stem cells promotes fracture healing in rats Cell Transplant 24 2643–55 [PubMed: 25647659]

[51]. Chowdhury E and Akaike T 2007 High performance DNA nano-carriers of carbonate apatite: Multiple factors in regulation of particle synthesis and transfection efficiency Int. J. Nanomed 2 101

[52]. Bitar M, Brown RA, Salih V, Kidane AG, Knowles JC and Nazhat SN 2008 Effect of cell density on osteoblastic differentiation and matrix degradation of biomimetic dense collagen scaffolds Biomacromolecules 9 129–35 [PubMed: 18095652]

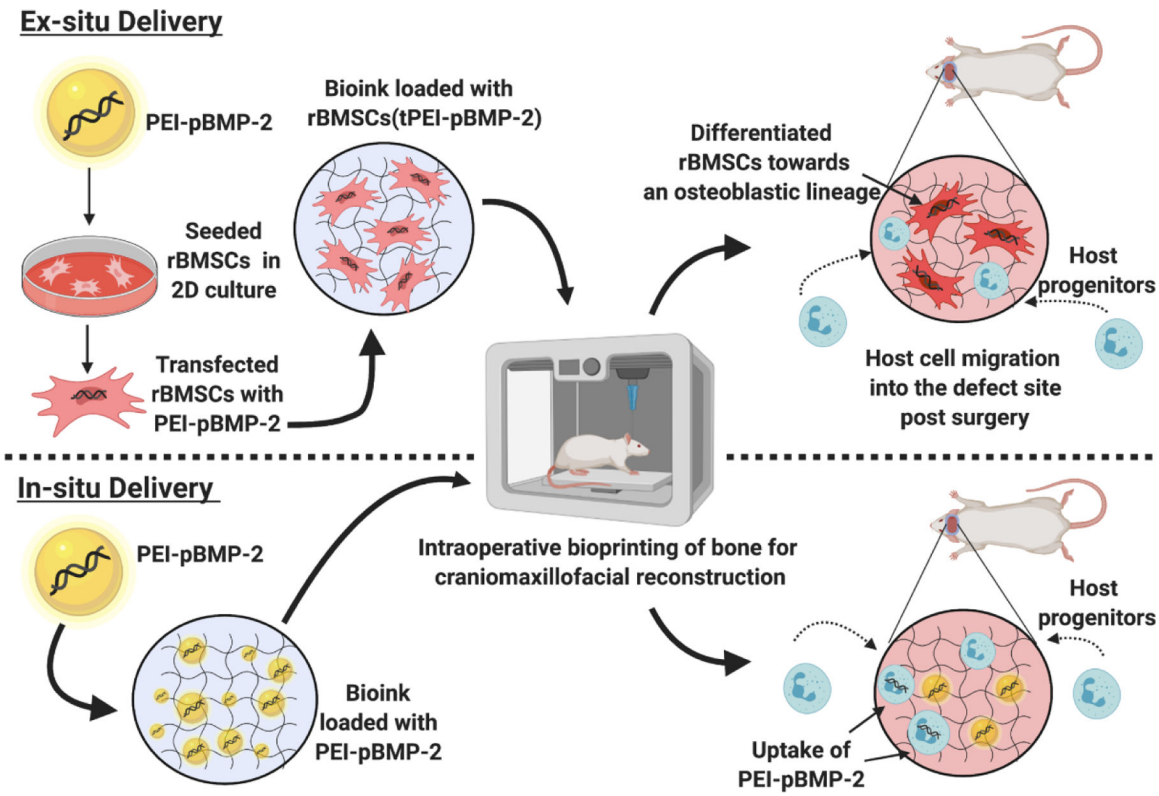

Figure 1.

(A) A schematic image of elucidating for ex-situ and in-situ delivery of PEI-pBMP-2 into critical-sized rat calvarial defects via intraoperative bioprinting for bone tissue repair (this figure was created using BioRender (https://biorender.com).

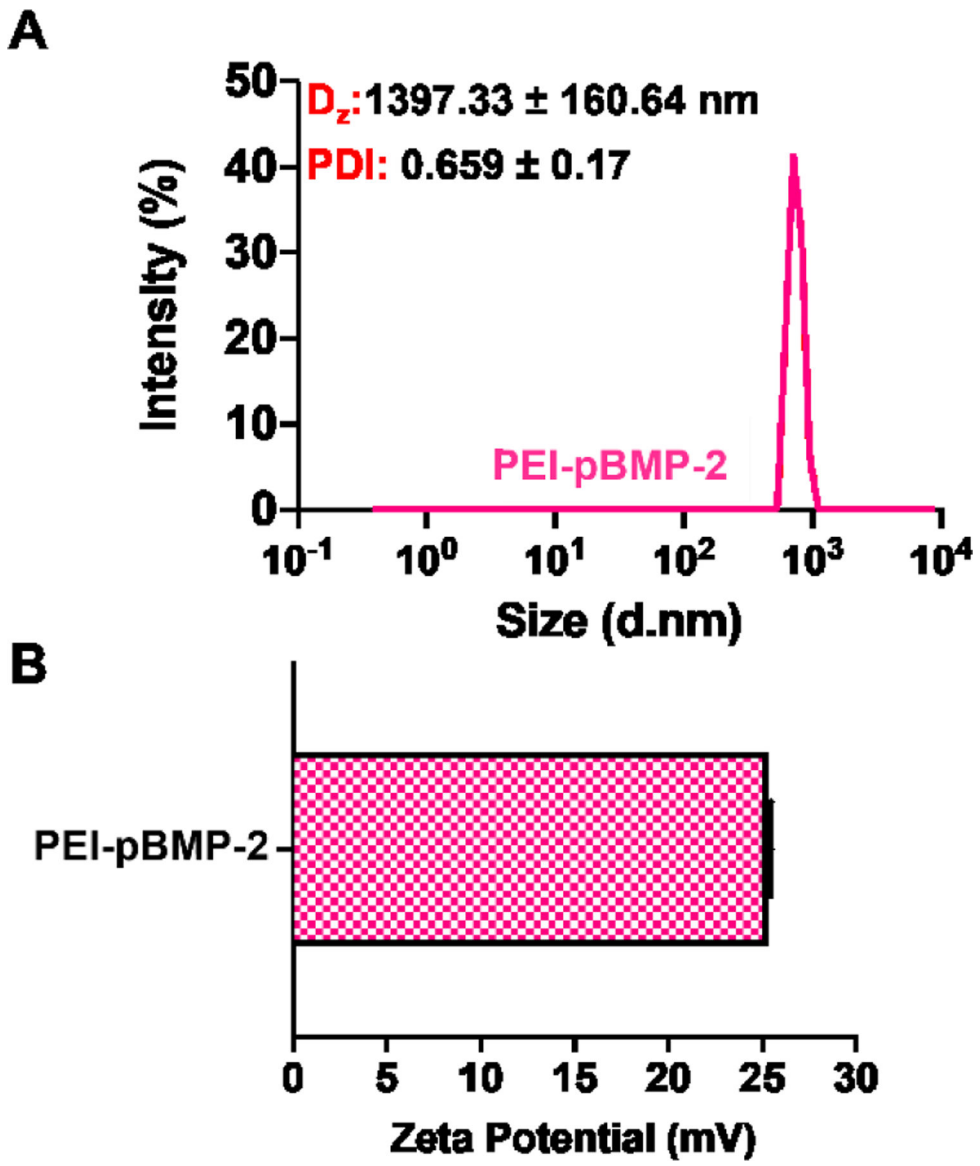

Figure 2.

(B) The particle size distribution and (C) zeta potential measurement of PEI-pBMP-2 complexes (n=3). Error bars indicate mean ± s.e.m.

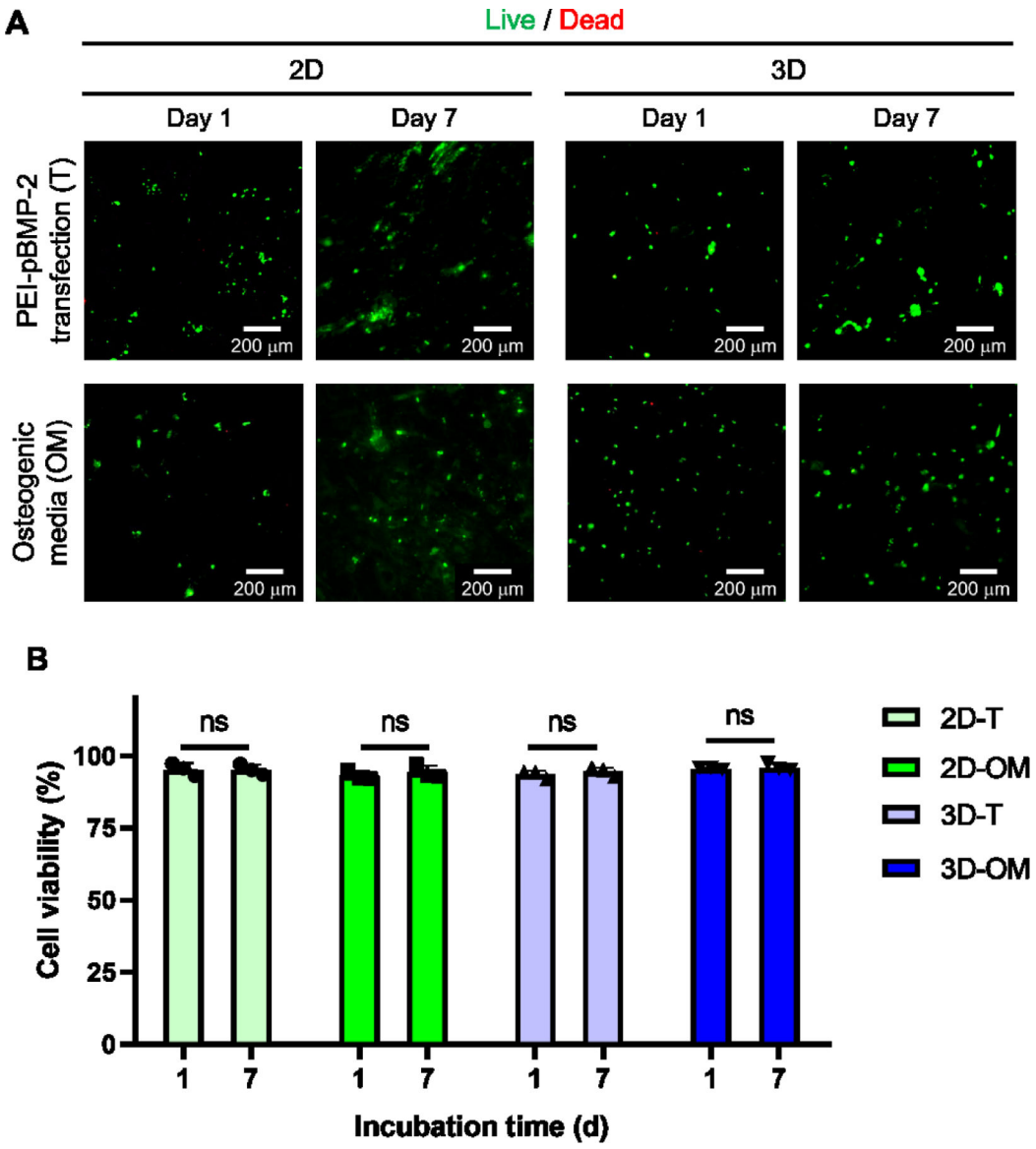

Figure 3.

(A) LIVE/DEAD images and (B) cell viability of hMSCs cultured in 2D and 3D at Days 1 and 7 (n=3, ns indicates non-significant).

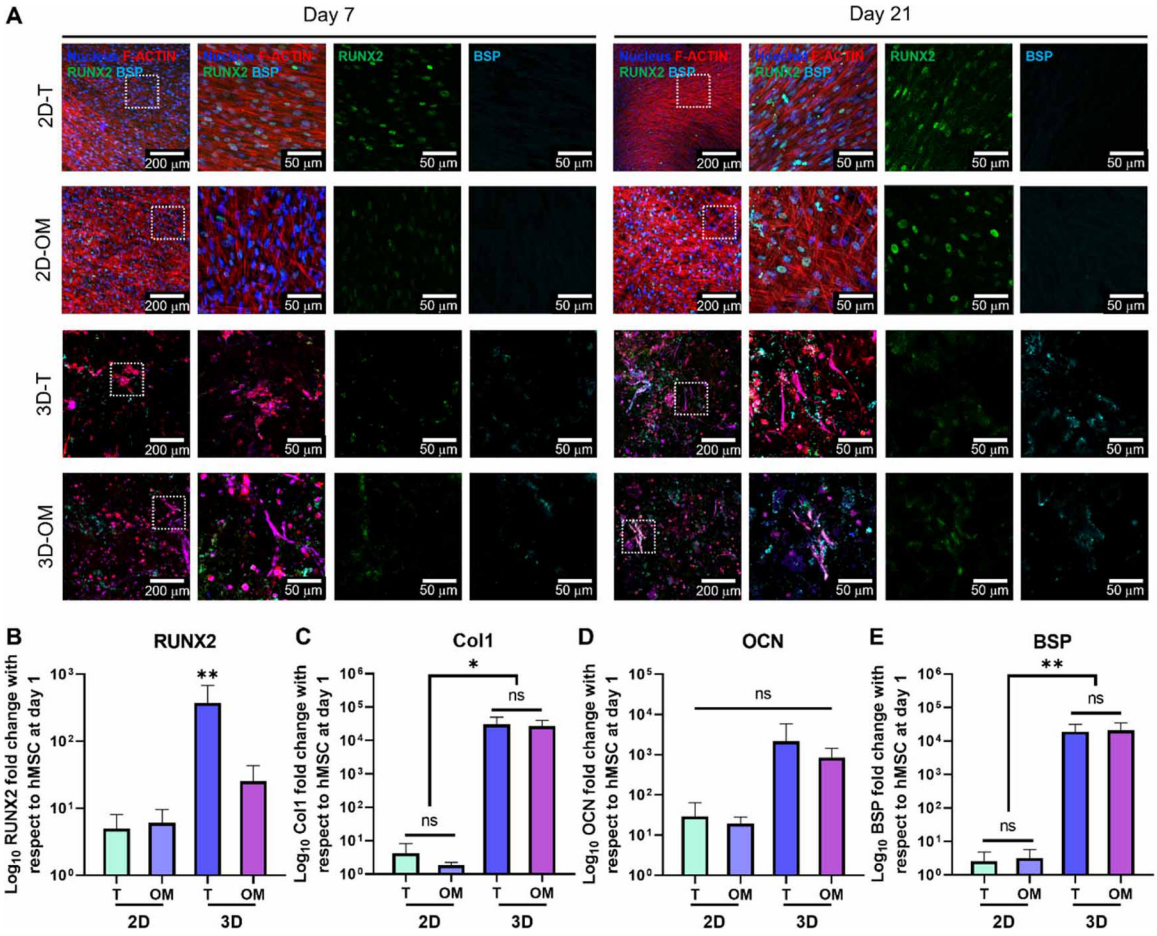

Figure 4.

(A) Immunofluorescent staining images demonstrating Hoechst, F-actin, RUNX2, and BSP of hMSCs cultured on 2D substrates and in 3D bioprinted constructs. RT-PCR measurement of osteogenic differentiation markers including (B) RUNX, (C) Col1, (D) OCN, and (E) BSP (n=3, *p<0.05, **p<0.01).

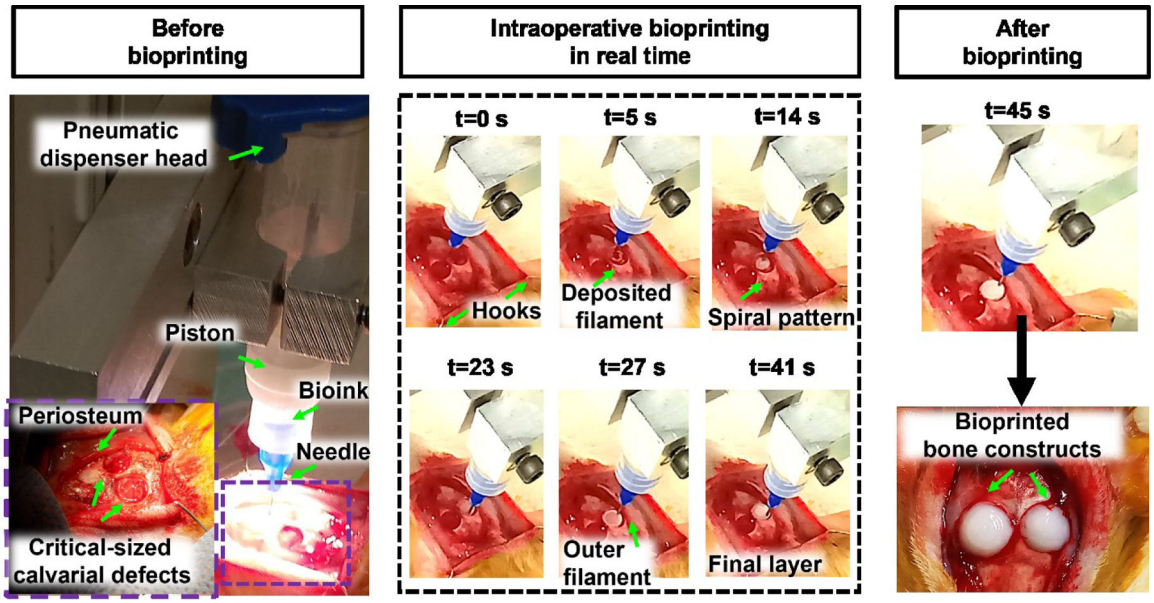

Figure 5.

Intraoperative bioprinting of bone before, during and after bioprinting using an extrusion-based system, where the animal was positioned under the bioprinter after opening two critical-sized calvarial defects. During the surgery, the periosteum was maintained intact. Next, the animal head was stabled using the hooks to avoid instant head movements during the IOB process. The bioprinting process initiated with the deposition of bioink after the positioning the print head at the start point of the calvarial defect. The bioink was directly extruded in a spiral pattern to deliver a 3D construct less than 1 min per defect. After filling both defects, the periosteum was sutured and then the skin was closed back.

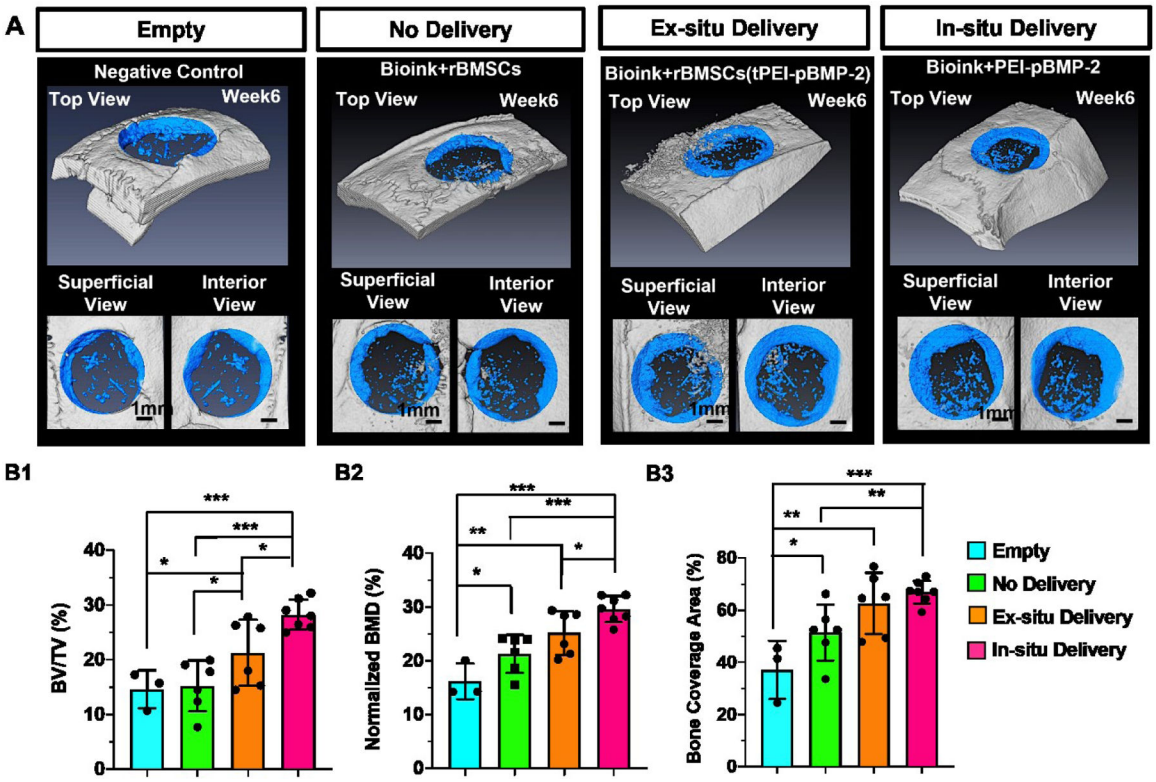

Figure 6.

(A) Determination of newly formed bone tissue in critical-sized rat calvarial defects using μCT scanning six weeks post surgery. Quantifications of (B1) BV/TV (%), (B2) normalized BMD (%) and (B3) bone coverage area (%) for empty (n=3), no delivery (n=6), ex-situ delivery (n=6) and in-situ delivery (n=7) groups. Data were expressed as mean ± s.d., $p^{*}<0.05$, $p^{**}<0.01$, and $p^{***}<0.001$.

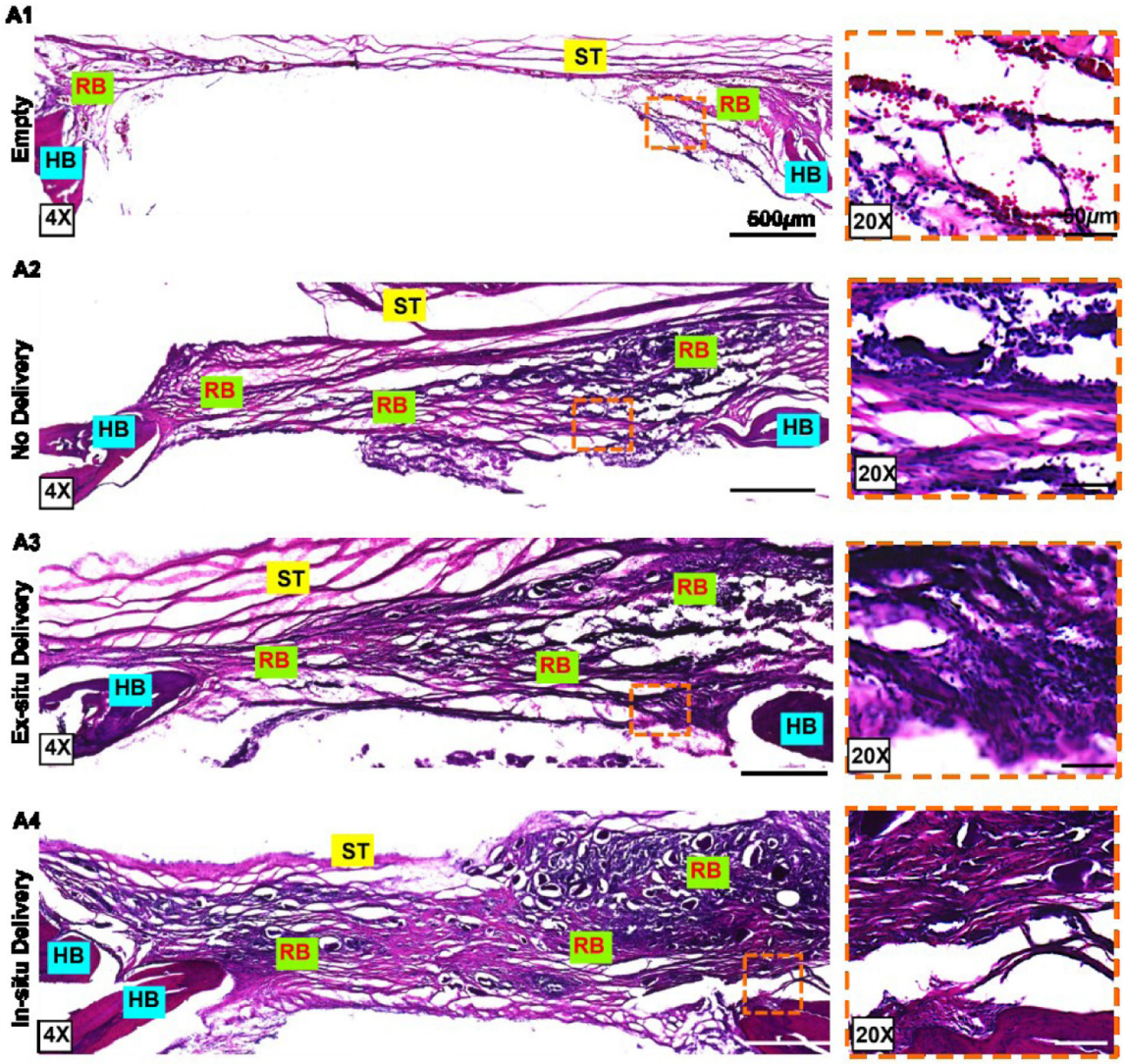

Figure 7.

Histomorphometric characterization of cryosectioned calvarial explants stained with H&E to determine bone tissue formation (HB: host bone; RB: regenerated bone; ST: soft tissue).

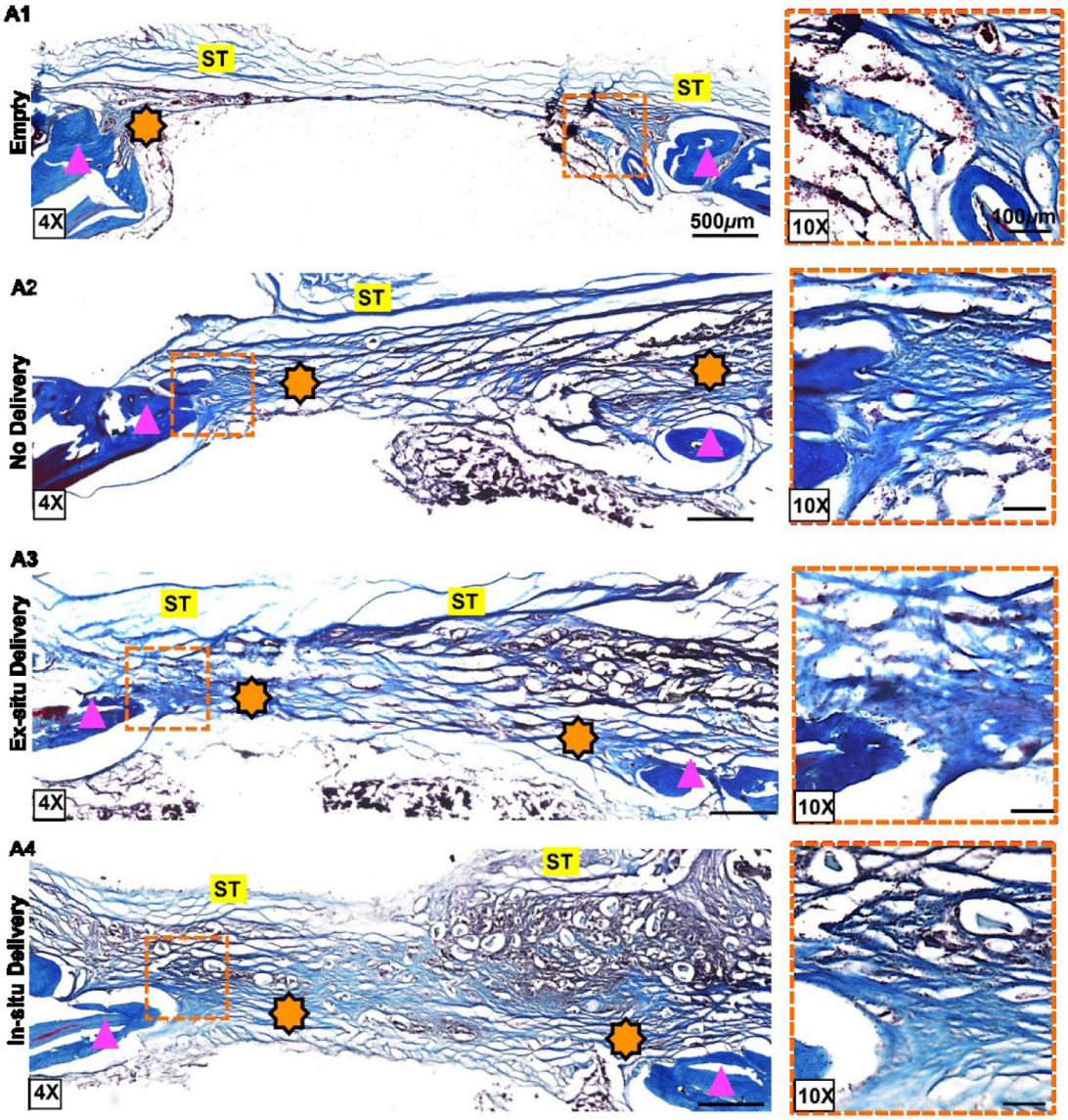

Figure 8.

MTS of cryosectioned calvarial explants for determination of bone tissue formation (ST: soft tissue; Triangle: mature bone; Star: immature bone).

Table 1.

Primers used for measuring osteogenic markers via RT-PCR.

Gene	Forward primer	Reverse primer
Col1	ATG ACT ATG AGT ATG GGG AAG CA	TGG GTC CCT CTG TTA CAC TTT
RUNX2	GGT TAA TCT CCG CAG GTC ACT	CAC TGT GCT GAA GAG GCT GTT
OCN	TCA CAC TCC TCG CCC TAT TG	TCG CTG CCC TCC TGC TTG
BSP	AAC GAA GAA AGC GAA GCA GAA	TCT GCC TCT GTG CTG TTG GT
GAPDH	CAC ATG GCC TCC AAG GAG TA	GTA CAT GAC AAG GTG CGG CT